A Mathematical Model for the Tooth Geometry of Hypoid Gears

C.-B. Tsay and J.-Y. Lin
Department of Mechanical Engineering, National Chiao Tung University
Hsinchu, Taiwan 30050, R.O.C.

Abstract—A mathematical model of the circular-cut hypoid gear set has been developed herein to represent the tooth surface geometry of hypoid gears. It can be applied to simulate the tooth profiles manufactured by the Duplex Method, Helical Duplex Method, and Formate Method. By applying the computer graphics and the proposed mathematical model, the profile of the hypoid gear and the precision coordinates of any tooth surface point can be obtained. The coordinates of the tooth surface can be considered as the standard for checking the profile precision of the actual products. The proposed mathematical model of the hypoid gear can also be applied to the computer numerical controlled (CNC) machining, tooth contact analysis (TCA), and finite element stress analysis.

NOMENCLATURE

A, B, C	Auxiliary function defined in equation (33)	**n**	Surface unit normal vector
a_{ij}	Auxiliary function defined in equation (14) ($i = 1, \ldots, 3$, $j = 1, \ldots, 3$)	O_d	Machine center, as shown in Figure 4b
b_{ij}	Auxiliary function defined in equation (22) ($i = 1, \ldots, 3$, $j = 1, \ldots, 4$)	O_d'	Crossing point of the vertical projection of the axes of two mating gears, as shown in Figure 4b
D_x	Work head setting, increment of machine center to back, as shown in Figure 4b	O_e	Pitch apex, as shown in Figure 4b
E_s	Sliding base movement, E_s is equal to the sliding base setting minus helical motion movement, as shown in Figure 4c	PAB	Distance measured from the crossing point of the vertical projection of the axes of mating gears to the pitch apex of the gear
E_v	Vertical offset of the work head with respect to the machine center, as shown in Figure 4c	Q	Basic cradle angle, as shown in Figure 2
L	Machine eccentric constant. $L = 3$ inches for Gleason #106 hypoid generator, and $L = 4.875$ inches for Gleason #122 hypoid generator	R_m	Nominal cutter radius, as shown in Figure 1a
		S_a	Coordinate system rigidly attached to the face mill cutter with axis Z_a coincides with the rotational axis of the face mill cutter, as shown in Figure 1b
$\frac{L}{2\pi}$	Helical motion of the sliding base per radian	S_b	Coordinate system rigidly attached to the fixed frame of the machine base (cradle housing), as shown in Figure 4a

Typeset by $\mathcal{A}_{\mathcal{M}}\mathcal{S}$-TEX

S_d — Coordinate system rigidly attached to the work spindle housing (gear blank housing), as shown in Figure 4b

S_e — Coordinate system rigidly attached to the workpiece (gear blank), as shown in Figure 4b

S_o — Coordinate system rigidly attached to the cradle, as shown in Figure 4a

S_s — Coordinate system rigidly attached to the cutter blade, as shown in Figure 1a

T_i — Roll ratio of change gear $(i = a, b, c, d)$

T_j — Helical motion of change gear $(j = e, f, g, h)$

u_i, u_o — Surface coordinates of the normal section of the straight-edged cutter blade, as shown in Figure 1b

$\mathbf{V}$ — Velocity vector

W — Point width of the face mill cutter, as shown in Figure 1a

X_b — Sliding base setting

β — Surface coordinate of the face mill cutter, as shown in Figure 1b

θ_i, θ_o — Surface coordinates of the tip fillet of cutter blade normal section, as shown in Figure 1b

ϵ — Wedge angle, as shown in Figure 3; $\epsilon = 15°$ for the Gleason #106 and #122 hypoid generators

η_a — Ratio of roll angles for the cradle and gear blank during generation process

ζ_c — Cradle rotation angle of the gear blank during generation process, as shown in Figure 4a

ζ_w — Work head rotation angle during generation process, as shown in Figure 4b

ρ_i, ρ_o — Tip fillet radii of the cutter blade normal section, as shown in Figure 1b

ψ_i, ψ_o — Pressure angle of the cutter blade, as shown in Figure 1b

ω_c — Angular velocity of the cradle in cutting process

ω_g — Angular velocity of the work piece in cutting process

ϕ_c — Cradle angle setting, as shown in Figure 2

ϕ_e — Eccentric angle setting, as shown in Figure 2

ϕ_s — Swivel angle setting, as shown in Figure 3

ϕ_t — Cutter spindle rotation angle setting, as shown in Figure 3

γ_m — Machine root angle setting, as shown in Figure 4c

τ — Auxiliary function defined in equation (14)

1. INTRODUCTION

Hypoid gear set is a primary element widely used by the industry to transmit the torque between crossed axes. In the past, since the precision coordinates of the hypoid gear profile had not been well developed, experimental testing was the only method used by the industry for the tooth contact analysis (TCA) and stress analysis. The experimental testing was time consuming and expensive. In this paper, a mathematical model for the complete hypoid gear profile is developed. It can be applied to the computer-aided tooth contact analysis (TCA), kinematic error analysis, stress analysis, dynamics analysis, and tooth geometry optimization of the hypoid gear.

Hypoid gears are similar to bevel gears, but with a shaft offset. Some important investigations related to the spiral bevel gear have been studied in recent years. Litvin and Gutman [1] proposed a method of synthesis and analysis for the "Formate" and "Helixform" hypoid gear in 1981. Wilcox [2] developed a method to calculate the stresses of the bevel and hypoid gear teeth in 1982. Huston et al. [3] made a tooth profile analysis of circular-cut spiral bevel gears in 1983. Litvin et al. [4] proposed a method for generation of spiral bevel gears based on the parallel motion of a straight line that slides along two mating ellipses in 1987. Litvin et al. [5] also presented the determination of tool settings of a tilted head cutter for the generation of hypoid and spiral bevel gears in 1988. Fong [6] presented the TCA and optimization of spiral bevel gears in 1990. Fong and Tsay [7,8] proposed a mathematical model for the tooth geometry of circular-cut spiral bevel gears in 1991.

In this paper, based on the theory of gearing [9], a mathematical model of the circular-cut hypoid gear set has been developed to simulate the widely used Gleason type circular-cut hypoid gear generators. The complete tooth geometry of the circular-cut hypoid gear has been mathe-

matically modeled. The mathematical model of the hypoid gear proposed herein can also cover the model of the spiral bevel gear developed by Fong and Tsay [7,8]. The proposed mathematical model includes the active tooth surfaces, fillet surfaces, bottom land, top land, face cone, and back cone of the hypoid gear tooth surfaces. It can be applied to simulate both the generated and nongenerated manufacturing methods, and can also be applied to the computer-aided TCA and finite element stress analysis.

2. EQUATIONS FOR THE HYPOID GEAR TOOTH PROFILES

Derivation of the equations for the hypoid gear tooth profiles can be divided into four main modules as follows:

(1) *Equations for the face mill cutter blade.* Generally, at the normal section of the head cutter blade, there are two straight-edged and two circular-arc as shown in Figure 1. For any other types of cutter blades, one can modify the corresponding equations of the cutter blade in this module.

(2) *Equations for the cradle set-up.* If four angles on the cradle including the cradle angle ψ_c, eccentric angle ψ_e, swivel angle ψ_s and cutter spindle rotation angle ψ_t are set-up, the tilted mechanism of the imaginary generating hypoid gear can be simulated to generate the hypoid gear that is located at the work head.

(3) *Equations of the spatial relations between the cradle and gear blank.* The geometric mechanism of the cradle and work head can be established in this module. Some different generating methods investigated herein include: (a) Formate (nongenerated) and Duplex (generated) methods, (b) helical motion of the work head during cutting process.

(4) *Equation of meshing.* Based on the theory of gearing, this module is needed for the generating process. If nongenerated method is adopted, this module is omitted.
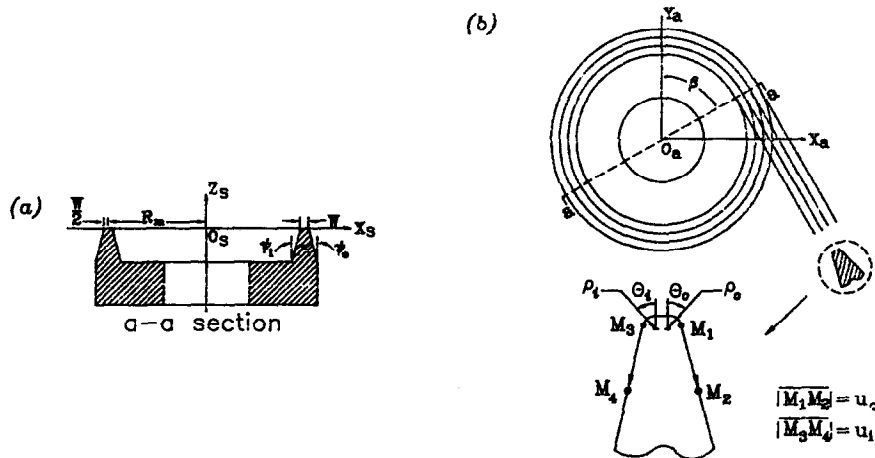

Figure 1. Normal section of the head cutter blade.

For simplicity, the following assumptions are made during the derivation process of the mathematical model:

(1) No elastic deformation is considered. In other words, rigid body motion is assumed during the cutting process.

(2) Neither dynamics loading nor temperature effect is considered.

(3) All the machine settings are precisely set-up. The tolerances and clearances of the hypoid gear generator are ignored.

3. THE GLEASON FACE MILL CUTTER

The normal section of the head cutter blade is represented in Figure 1a, and the enlarged section of the cutter blade is shown in Figure 1b. The normal section of the cutter blade consists

of two circular-arc and two straight-edged. Parameters θ_i and θ_o are the surface coordinates of the inside and outside circular-arc of the cutter blade, respectively. Parameters u_i and u_o are the surface coordinates of the inside and outside straight-edged of the cutter blade, respectively. According to these four parameters, the equations of the cutter blade at the normal section can be represented in the coordinate system S_s (X_s , Y_s , Z_s) as follows.

(a) Equations of the inside and outside circular-arc portions are

$$
\begin{aligned}
X_s^{fi} &= R_m - \frac{W}{2} + \rho_i \left(\frac{1 - \sin \psi_i}{\cos \psi_i} \right) - \rho_i \sin \theta_i \\
Y_s^{fi} &= 0 \\
Z_s^{fi} &= -\rho_i(1 - \cos \theta_i),
\end{aligned}
\tag{1}
$$

and

$$
\begin{aligned}
X_s^{fo} &= R_m + \frac{W}{2} - \rho_o \left(\frac{1 - \sin \psi_o}{\cos \psi_o} \right) + \rho_o \sin \theta_o \\
Y_s^{fo} &= 0 \\
Z_s^{fo} &= -\rho_o(1 - \cos \theta_o).
\end{aligned}
\tag{2}
$$

(b) Equations of the inside and outside straight-edged portion are

$$
\begin{aligned}
X_s^{i} &= R_m - \frac{W}{2} - \rho_i \left(\frac{1 - \sin \psi_i}{\cos \psi_i} \right) \sin \psi_i - U_i \sin \psi_i \\
Y_s^{i} &= 0 \\
Z_s^{i} &= -\rho_i(1 - \sin \psi_i) - U_i \cos \psi_i,
\end{aligned}
\tag{3}
$$

and

$$
\begin{aligned}
X_s^{o} &= R_m + \frac{W}{2} + \rho_o \left(\frac{1 - \sin \psi_0}{\cos \psi_o} \right) \sin \psi_o + U_o \sin \psi_o \\
Y_s^{o} &= 0 \\
Z_s^{o} &= -\rho_o(1 - \sin \psi_o) - U_o \cos \psi_o.
\end{aligned}
\tag{4}
$$

where superscripts "fi" and "fo" indicate the inside and outside circular-arc, respectively, super-scripts "i" and "o" indicate the inside and outside straight-edged, respectively, and subscript "s" indicates that the equations are represented in coordinate system S_s (X_s, Y_s, Z_s). Parameters ψ_i and ψ_o indicate the pressure angles of the inside and outside straight-edged, respectively, while ρ_i and ρ_o indicate the radii of the inside and outside circular-arc, respectively, R_m is the cutter radius, and W is the point width of the cutter blade as shown in Figure 1.

The equations of the head cutter can be represented in coordinate system S_a (X_a, Y_a, Z_a) by rotating the normal section of the cutter blade along the axis Z_a through a rotation angle β as shown in Figure 1b. By applying the transformation matrix equation, the equations of the cutter blade represented in coordinate system S_s (X_s, Y_s, Z_s) can be transformed into coordinate system S_a (X_a, Y_a, Z_a) as follows:

$$
\begin{bmatrix} X_a \\ Y_a \\ Z_a \end{bmatrix} = \begin{bmatrix} \sin \beta & -\cos \beta & 0 \\ \cos \beta & \sin \beta & 0 \\ 0 & 0 & 1 \end{bmatrix} \begin{bmatrix} X_s \\ Y_s \\ Z_s \end{bmatrix}.
\tag{5}
$$

Substituting equations (1) and (2) into equation (5), the inside and outside profiles of the head cutter for the circular-arc portion can be obtained as follows:

$$
\begin{aligned}
X_a^{fi} &= \left\{ R_m - \frac{W}{2} + \rho_i \left(\frac{1 - \sin \psi_i}{\cos \psi_i} \right) - \rho_i \sin \theta_i \right\} \sin \beta \\
Y_a^{fi} &= \left\{ R_m - \frac{W}{2} + \rho_i \left(\frac{1 - \sin \psi_i}{\cos \psi_i} \right) - \rho_i \sin \theta_i \right\} \cos \beta \\
Z_a^{fi} &= -\rho_i(1 - \cos \theta_i),
\end{aligned}
\tag{6}
$$

and

$$X_a^{fo} = \left\{ R_m + \frac{W}{2} - \rho_o \left(\frac{1 - \sin \psi_o}{\cos \psi_o} \right) + \rho_o \sin \theta_o \right\} \sin \beta$$

$$Y_a^{fo} = \left\{ R_m + \frac{W}{2} - \rho_o \left(\frac{1 - \sin \psi_o}{\cos \psi_o} \right) + \rho_o \sin \theta_o \right\} \cos \beta \qquad (7)$$

$$Z_a^{fo} = -\rho_o (1 - \cos \theta_o).$$

Similarly, by substituting equations (3) and (4) into equation (5), the inside and outside profiles of the head cutter of the straight-edged portion can be obtained as follows:

$$X_a^i = \left\{ R_m - \frac{W}{2} - \rho_i \left(\frac{1 - \sin \psi_i}{\cos \psi_i} \right) \sin \psi_i - U_i \sin \psi_i \right\} \sin \beta$$

$$Y_a^i = \left\{ R_m - \frac{W}{2} - \rho_i \left(\frac{1 - \sin \psi_i}{\cos \psi_i} \right) \sin \psi_i - U_i \sin \psi_i \right\} \cos \beta \qquad (8)$$

$$Z_a^i = -\rho_i (1 - \sin \psi_i) - U_i \cos \psi_i,$$

and

$$X_a^o = \left\{ R_m + \frac{W}{2} + \rho_o \left(\frac{1 - \sin \psi_o}{\cos \psi_o} \right) \sin \psi_o + U_o \sin \psi_o \right\} \sin \beta$$

$$Y_a^o = \left\{ R_m + \frac{W}{2} + \rho_o \left(\frac{1 - \sin \psi_o}{\cos \psi_o} \right) \sin \psi_o + U_o \sin \psi_o \right\} \cos \beta \qquad (9)$$

$$Z_a^o = -\rho_o (1 - \sin \psi_o) - U_o \cos \psi_o.$$

The surface unit normal vector of the head cutter is required for the derivation of the equation of meshing. Therefore, derivation of the surface unit normal vector of the head cutter should be performed herein. Based on equations (6) and (7), the surface unit normal vectors of inside and outside profiles of the head cutter circular-arc portion can be obtained as follows:

$$n_{xa}^{fi} = \sin \theta_i \sin \beta$$

$$n_{ya}^{fi} = \sin \theta_i \cos \beta \qquad (10)$$

$$n_{za}^{fi} = -\cos \theta_i,$$

and

$$n_{xa}^{fo} = -\sin \theta_o \sin \beta$$

$$n_{ya}^{fo} = -\sin \theta_o \cos \beta \qquad (11)$$

$$n_{za}^{fo} = -\cos \theta_o.$$

Similarly, based on equations (8) and (9), the surface unit normal vectors of the inside and outside profiles of the head cutter straight-edged portion can also be obtained as follows :

$$n_{xa}^i = \cos \psi_i \sin \beta$$

$$n_{ya}^i = \cos \psi_i \cos \beta \qquad (12)$$

$$n_{xa}^i = -\sin \psi_i,$$

and

$$n_{xa}^o = -\cos \psi_o \sin \beta$$

$$n_{ya}^o = -\cos \psi_o \cos \beta \qquad (13)$$

$$n_{xa}^o = -\sin \psi_o.$$

The notations of superscripts and subscripts represented in equations (10)–(13) are the same as those represented in equations (6)–(9).

4. THE GLEASON TILTED HEAD CUTTER

For the Gleason hypoid gear generator, the head cutter has to satisfy the specified tilted and declination during the tool setting process. Therefore, four adjustable angles at the cradle mechanism including cradle angle ψ_c, eccentric angle ψ_e, swivel angle ψ_s and cutter spindle rotation angle ψ_t are needed. The tilted cradle mechanism of the Gleason hypoid gear generator was analyzed by Litvin [5] in 1988. The relations of coordinate systems of the tilted cradle mechanism are shown in Figures 2 and 3. The corresponding homogeneous coordinate transformation matrix equation is shown below to transform the locus of the head cutter from coordinate system S_a to coordinate system S_o.

$$\begin{bmatrix} X_o \\ Y_o \\ Z_o \\ 1 \end{bmatrix} = \begin{bmatrix} a_{11} & a_{12} & a_{13} & a_{14} \\ a_{21} & a_{22} & a_{23} & a_{24} \\ a_{31} & a_{32} & a_{33} & 0 \\ 0 & 0 & 0 & 1 \end{bmatrix} \begin{bmatrix} X_a \\ Y_a \\ Z_a \\ 1 \end{bmatrix}, \tag{14}$$

where

$$a_{11} = \cos\tau \left(\cos^2\epsilon \cos\psi_t + \sin^2\epsilon\right) - \sin\tau \cos\epsilon \sin\psi_t$$

$$a_{12} = \cos\tau \cos\epsilon \sin\psi_t + \sin\tau \cos\psi_t$$

$$a_{13} = 0.5\left(1 - \cos\psi_t\right)\cos\tau \sin 2\epsilon + \sin\tau \sin\epsilon \sin\psi_t$$

$$a_{14} = L\left[\cos\psi_c - \cos(\psi_c + \psi_e)\right]$$

$$a_{21} = -\sin\tau \left(\cos^2\epsilon \cos\psi_t + \sin^2\epsilon\right) - \cos\tau \, cos\epsilon \, \sin\psi_t$$

$$a_{22} = -\sin\tau \cos\epsilon \sin\psi_t + \cos\tau \cos\psi_t$$

$$a_{23} = -0.5\left(1 - \cos\psi_t\right)\sin\tau \sin 2\epsilon + \cos\tau \sin\epsilon \sin\psi_t$$

$$a_{24} = -L\left[\sin\psi_c - \sin(\psi_c + \psi_e)\right]$$

$$a_{31} = 0.5\left(1 - \cos\psi_t\right)\sin 2\epsilon$$

$$a_{32} = -\sin\epsilon \sin\psi_t$$

$$a_{33} = \sin^2\epsilon \cos\psi_t + \cos^2\epsilon$$

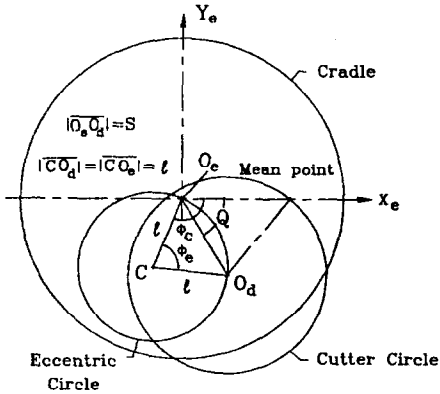$$\tau = \psi_c + \psi_e + \psi_s.$$

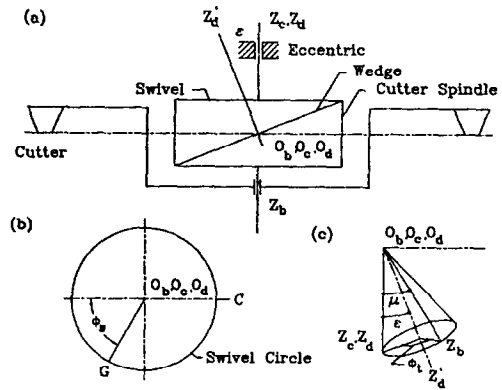Figure 2. Eccentric equipment assembly.   Figure 3. Tilted equipment assembly.

Similarly, the surface unit normal vector of the head cutter can also be represented in coordinate system S_o by applying the transformation matrix equation as follows:

$$\begin{bmatrix} n_{xo} \\ n_{yo} \\ n_{zo} \end{bmatrix} = \begin{bmatrix} a_{11} & a_{12} & a_{13} \\ a_{21} & a_{22} & a_{23} \\ a_{31} & a_{32} & a_{33} \end{bmatrix} \begin{bmatrix} n_{xa} \\ n_{ya} \\ n_{za} \end{bmatrix}. \tag{15}$$

5. MECHANISM OF THE GLEASON HYPOID GEAR GENERATOR

The geometric mechanism of the Gleason hypoid gear generator [10] is shown in Figure 4. The generator is available to both the generated and nongenerated hypoid gear manufacturing methods. As shown in Figure 4a, coordinate systems S_b and S_o are attached to the cradle housing and cradle, respectively. The angle ζ_c is the rotation angle of the cradle with respect to the cradle housing. In Figure 4b, coordinate systems S_d and S_e are attached to the gear blank housing and gear blank, respectively. The angle ζ_w is the rotation angle of the gear blank with respect to the gear blank housing. The geometric relation between the cradle housing and gear blank housing is shown in Figure 4c. The relation between rotation angles ζ_c and ζ_w is related by:

$$\zeta_w = \zeta_c \times \left[\left(\frac{T_a}{T_b} \times \frac{T_c}{T_d}\right) \times \frac{50}{T_n}\right], \tag{16}$$

where T_a, T_b, T_c, and T_d are the Nc/50 ratio gears, and they should follow the data given by the Gleason hypoid gear generator (Refer to Table 1), and T_n represents the teeth number of the generated gear.
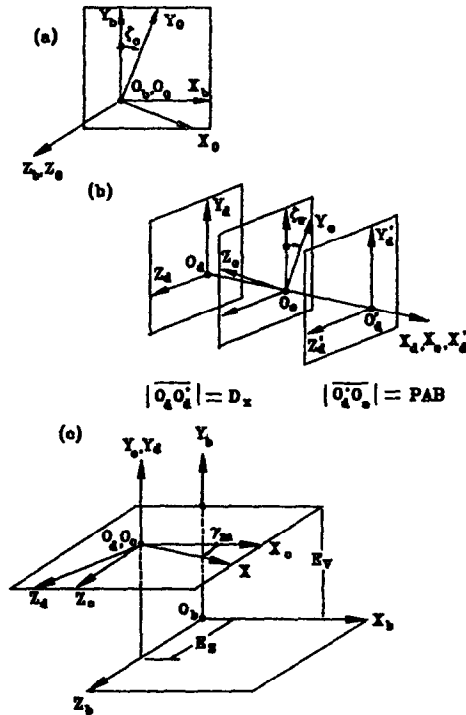

Figure 4. Coordinate systems for the mechanism of Gleason hypoid generator.

Based on the relation of the coordinate systems shown in Figure 3, the locus of the head cutter can be represented in the coordinate system S_e. The homogeneous coordinate transformation matrix equations are obtained as follows:

$$\begin{bmatrix} X_b \\ Y_b \\ Z_b \\ 1 \end{bmatrix} = \begin{bmatrix} \cos\zeta_c & \sin\zeta_c & 0 & 0 \\ -\sin\zeta_c & \cos\zeta_c & 0 & 0 \\ 0 & 0 & 1 & 0 \\ 0 & 0 & 0 & 1 \end{bmatrix} \begin{bmatrix} X_o \\ Y_o \\ Z_o \\ 1 \end{bmatrix} \tag{17}$$

$$\begin{bmatrix} X_d \\ Y_d \\ Z_d \\ 1 \end{bmatrix} = \begin{bmatrix} \cos\gamma_m & 0 & \sin\gamma_m & -E_s\sin\gamma_m \\ 0 & 1 & 0 & -E_v \\ -\sin\gamma_m & 0 & \cos\gamma_m & -E_s\cos\gamma_m \\ 0 & 0 & 0 & 1 \end{bmatrix} \begin{bmatrix} X_b \\ Y_b \\ Z_b \\ 1 \end{bmatrix} \tag{18}$$

$$\begin{bmatrix} X'_d \\ Y'_d \\ Z'_d \\ 1 \end{bmatrix} = \begin{bmatrix} 1 & 0 & 0 & -D_x \\ 0 & 1 & 0 & 0 \\ 0 & 0 & 1 & 0 \\ 0 & 0 & 0 & 1 \end{bmatrix} \begin{bmatrix} X_d \\ Y_d \\ Z_d \\ 1 \end{bmatrix} \tag{19}$$

$$\begin{bmatrix} X_e \\ Y_e \\ Z_e \\ 1 \end{bmatrix} = \begin{bmatrix} 1 & 0 & 0 & PAB \\ 0 & \cos\zeta_w & -\sin\zeta_w & 0 \\ 0 & \sin\zeta_w & \cos\zeta_w & 0 \\ 0 & 0 & 0 & 1 \end{bmatrix} \begin{bmatrix} X'_d \\ Y'_d \\ Z'_d \\ 1 \end{bmatrix}. \tag{20}$$

In order to present a completed tooth profile of the hypoid gear, a new coordinate system S'_d is needed as shown in Figure 4b. Symbol O_d is the machine center, O'_d is the crossing point of the axes of mating gears on the vertical projection, and O_e is the pitch apex. Parameter E_s is the sliding base movement and can be expressed by

$$E_s = X_b - \left(\frac{L}{2\pi}\right)\zeta_c, \tag{21}$$

where X_b is the initial position of the sliding base, and $\left(\frac{L}{2\pi}\right)$ is the linear translation of the work head (i.e., helical motion) per radian of the cradle roll. The value of $\left(\frac{L}{2\pi}\right)$ is given by

$$\frac{L}{2\pi} = 0.083075889\,{}^* \left[\frac{T_e}{T_f} \times \frac{T_g}{T_h}\right] \text{ inches for the Gleason \#106}$$

hypoid gear generator

$$\frac{L}{2\pi} = 0.313803110\,{}^* \left[\frac{T_e}{T_f} \times \frac{T_g}{T_h}\right] \text{ inches for the Gleason \#122}$$

hypoid gear generator,

where T_e, T_f, T_g, and T_h are the helical motion gears, and they should follow the data given by the Gleason hypoid gear generator (refer to Table 1). Other types of Gleason hypoid gear generators have different values of $\frac{L}{2\pi}$. Parameter E_v is the blank offset, D_x is the increment of the machine center to the back, PAB is the distance measured from the crossing point of the axes of mating gears on the vertical projection to the pitch apex of the gear, and γ_m is the machine root angle.

When the distance $|\overline{O'_d O_d}|$ is set to zero $(PAB = 0)$, the proposed mathematical model of hypoid gears becomes a mathematical model of spiral bevel gears. In other words, the mathematical model of spiral bevel gears is a special case of the herein proposed mathematical model of hypoid gears.

Equations (17)–(20) can be rearranged and simplified as follows:

$$\begin{bmatrix} X_e \\ Y_e \\ Z_e \\ 1 \end{bmatrix} = \begin{bmatrix} b_{11} & b_{12} & b_{13} & b_{14} \\ b_{21} & b_{22} & b_{23} & b_{24} \\ b_{31} & b_{32} & b_{33} & b_{34} \\ 0 & 0 & 0 & 1 \end{bmatrix} \begin{bmatrix} X_o \\ Y_o \\ Z_o \\ 1 \end{bmatrix} \tag{22}$$

$$b_{11} = \cos\gamma_m \cos\zeta_c$$

$$b_{12} = \cos\gamma_m \sin\zeta_c$$

$$b_{13} = \sin\gamma_m$$

$$b_{14} = -\left(x_b - \frac{L}{2\pi}\zeta_c\right)\sin\gamma_m - (D_x - PAB)$$

$$b_{21} = \sin\zeta_w \sin\gamma_m \cos\zeta_c - \cos\zeta_w \sin\zeta_c$$

$$b_{22} = \sin\zeta_w \sin\gamma_m \sin\zeta_c + \cos\zeta_w \cos\zeta_c$$

$$b_{23} = -\sin\zeta_w \, \cos\gamma_m$$

$$b_{24} = -E_v \cos\zeta_w + \left(x_b - \frac{L}{2\pi}\zeta_c\right)\sin\zeta_w \, \cos\gamma_m$$

$$b_{31} = -\cos\zeta_w \sin\gamma_m \, \cos\zeta_c - \sin\zeta_w \, \sin\zeta_c$$

$$b_{32} = -\cos\zeta_w \sin\gamma_m \, \sin\zeta_c + \sin\zeta_w \, \cos\zeta_c$$

$$b_{33} = \cos\zeta_w \, \cos\gamma_m$$

$$b_{34} = -E_v \sin\zeta_w - \left(x_b - \frac{L}{2\pi}\zeta_c\right)\cos\zeta_w \, \cos\gamma_m.$$

Equation (22) expresses the locus of the head cutter represented in coordinate system S_e, and coordinates of X_o, Y_o, and Z_o are given and expressed in equation (14).

6. EQUATION OF MESHING

During the generating process, the generating surface of the head cutter tool and the generated surface of the gear blank are always in tangency, and the relative velocity of these two surfaces is lain on the common tangent plane. Since at the line of common contact, the surface common unit normal vector is perpendicular to the common tangent plane, the following equation must be satisfied [9]:

$$\mathbf{n}_b \cdot \mathbf{V}_b^{cg} = 0, \tag{23}$$

where $\mathbf{n}_b$ is the unit normal vector of the generating surface, and $\mathbf{V}_b^{cg}$ is the relative velocity of the generating tool surface with respect to the generated gear blank surface. Subscript "b" indicates that both vectors $\mathbf{n}_b$ and $\mathbf{V}_b^{cg}$ are represented in the coordinate system S_b. Equation (23) is the so-called "equation of meshing" in the theory of gearing. It relates the rotation angle of the cradle ζ_c to the surface coordinates u_i and β (or u_o and β) of generating cutter at the straight-edged portion, and θ_i and β (or θ_o and β) at the circular-arc portion. The relative velocity $\mathbf{V}_b^{cg}$ can be obtained as follows:

$$\mathbf{V}_b^{cg} = \mathbf{V}_b^c - \mathbf{V}_b^g, \tag{24}$$

where

$$\mathbf{V}_b^c = \mathbf{\Omega}_c \times \mathbf{R}_c$$
$$= \begin{bmatrix} \mathbf{i} & \mathbf{j} & \mathbf{k} \\ 0 & 0 & -\omega_c \\ X_b & Y_b & Z_b \end{bmatrix} = \omega_c \, Y_b \, \mathbf{i} - \omega_c \, X_b \, \mathbf{j}, \tag{25}$$

and

$$\mathbf{V}_b^g = \mathbf{\Omega}_g \times \mathbf{R}_g + \frac{L}{2\pi}\,\omega_c\,\mathbf{k}$$
$$= \begin{bmatrix} \mathbf{i} & \mathbf{j} & \mathbf{k} \\ -\omega_g \cos\gamma_m & 0 & -\omega_g \sin\gamma_m \\ X_b & Y_b - E_v & Z_b - E_s \end{bmatrix} + \frac{L}{2\pi}\,\omega_c\,\mathbf{k}$$
$$= \omega_g(Y_b - E_v)\sin\gamma_m \, \mathbf{i} - [\omega_g \, X_b \sin\gamma_m - \omega_g \, (Z_b - E_s)\cos\gamma_m]\,\mathbf{j}$$
$$\quad + \left[\omega_g(Y_b - E_v)\cos\gamma_m + \frac{L}{2\pi}\,\omega_c\right]\mathbf{k}. \tag{26}$$

Let

$$\eta_a(\zeta_c) = \frac{\omega_g}{\omega_c} = \frac{\zeta_w}{\zeta_c}, \tag{27}$$

and substituting equations (25)–(27) into equation (24), the relative velocity $\mathbf{V}_b^{cg}$ becomes

$$\mathbf{V}_b^{cg} = -\omega_c \begin{bmatrix} (Y_b - E_v)\,\eta_a \sin\gamma_m - Y_b \\ X_b(1 - \eta_a \sin\gamma_m) + (Z_b - E_s)\,\eta_a \cos\gamma_m \\ -(Y_b - E_v)\,\eta_a \cos\gamma_m - \frac{L}{2\pi} \end{bmatrix}, \tag{28}$$

where X_b, Y_b, and Z_b are the surface coordinates of the head cutter represented in coordinate system S_b, and they can be obtained by applying the coordinate transformation matrix equation (Figure 4a):

$$\begin{bmatrix} X_b \\ Y_b \\ Z_b \end{bmatrix} = \begin{bmatrix} \cos\zeta_c & \sin\zeta_c & 0 \\ -\sin\zeta_c & \cos\zeta_c & 0 \\ 0 & 0 & 1 \end{bmatrix} \begin{bmatrix} X_o \\ Y_o \\ Z_o \end{bmatrix} = \begin{bmatrix} X_o\cos\zeta_c + Y_o\sin\zeta_c \\ -X_o\sin\zeta_c + Y_o\cos\zeta_c \\ Z_o \end{bmatrix}, \qquad (29)$$

where X_o, Y_o, and Z_o are the position coordinates represented in equation (14).

The unit normal vector $\mathbf{n}_b$ can also be obtained by applying the similar transformation matrix equation:

$$\begin{bmatrix} n_{xb} \\ n_{yb} \\ n_{zb} \end{bmatrix} = \begin{bmatrix} \cos\zeta_c & \sin\zeta_c & 0 \\ -\sin\zeta_c & \cos\zeta_c & 0 \\ 0 & 0 & 1 \end{bmatrix} \begin{bmatrix} n_{xo} \\ n_{yo} \\ n_{zo} \end{bmatrix} = \begin{bmatrix} n_{xo}\cos\zeta_c + n_{yo}\sin\zeta_c \\ -n_{xo}\sin\zeta_c + n_{yo}\cos\zeta_c \\ n_{zo} \end{bmatrix}, \qquad (30)$$

where n_{xo}, n_{yo}, and n_{zo} are the components of the surface unit normal vector of the head cutter represented in equation (15).

By substituting equations (28)–(30) into equation (23), the equation of meshing is thus obtained as follows:

$$\begin{aligned} \mathbf{n}_b \cdot \mathbf{V}_b^{cg} = {}& (n_{xo}\cos\zeta_c + n_{yo}\sin\zeta_c)\,[(\eta_a\sin\gamma_m - 1)Y_b - \eta_a\,E_v\sin\gamma_m] \\ &+ (-n_{xo}\sin\zeta_c + n_{yo}\cos\zeta_c)[(1 - \eta_a\sin\gamma_m)X_b - \eta_a\,(Z_b - E_s)\cos\gamma_m] \\ &- n_{zo}\,\eta_a(Y_b - E_v)\cos\gamma_m - n_{zo}\frac{L}{2\pi} \\ = {}& 0. \end{aligned} \qquad (31)$$

If both sides of equation (31) are divided by η_a and let $K = \left(\sin\gamma_m - \frac{1}{\eta_a}\right)$, then equation (31) becomes

$$\begin{aligned} &(n_{xo}\cos\zeta_c + n_{yo}\sin\zeta_c)\,[K\,(-X_o\sin\zeta_c + Y_o\cos\zeta_c) - E_v\sin\gamma_m] \\ &+ (n_{xo}\sin\zeta_c - n_{yo}\cos\zeta_c)\,[K\,(X_o\cos\zeta_c + Y_o\sin\zeta_c) - (Z_b - E_s)\cos\gamma_m] \\ &+ n_{zo}\,E_v\cos\gamma_m - n_{zo}\,(-X_o\sin\zeta_c + Y_o\cos\zeta_c)\cos\gamma_m - \frac{n_{zo}}{\eta_a}\frac{L}{2\pi} \\ &= 0. \end{aligned} \qquad (32)$$

Equation (32) can also be simplied as follows:

$$\mathbf{A} + \mathbf{B}\sin\zeta_c + \mathbf{C}\cos\zeta_c = 0, \qquad (33)$$

where

$$\mathbf{A} = \left(\sin\gamma_m - \frac{1}{\eta_a}\right)(Y_o\,n_{xo} - X_o\,n_{yo}) + n_{zo}\,E_v\cos\gamma_m - \frac{n_{zo}}{\eta_a}\frac{L}{2\pi}$$
$$\mathbf{B} = -E_v\,n_{yo}\sin\gamma_m - [n_{xo}(Z_o - E_s) - X_o\,n_{zo}]\cos\gamma_m$$
$$\mathbf{C} = -E_v\,n_{xo}\sin\gamma_m + [n_{yo}(Z_o - E_s) - Y_o\,n_{zo}]\cos\gamma_m.$$

It is noticed that X_o, Y_o, and Z_o are expressed in equation (14), and n_{xo}, n_{yo}, and n_{zo} are represented in equation (15). Equation (33) is the equation of meshing for the hypoid gears. The gear tooth surfaces of the generated hypoid gear can be obtained by considering the equation of meshing and the locus of the head cutter simultaneously. Therefore, equations (22) and (33) define the tooth surface of the hypoid gear. The data of the right-hand hypoid pinion and left-hand hypoid gear given by the Gleason Works are listed in Table 1. By applying the computer graphics and proposed mathematical model represented by equations (22) and (33), the tooth profiles of the hypoid pinion and gear can be plotted and shown in Figures 5 and 6, respectively.

Table 1. Data for Example 1.

| Items	Pinion	Gear
Teeth number	6	40
Face angle	13° 26′	80° 41′
Pitch angle	9° 59′	79° 55′
Outer cone dist.	155.55 mm	159.46 mm
Face width	44.92 mm	42.00 mm
Outside addendum	9.90 mm	1.35 mm
Outside dedendum	3.00 mm	11.45 mm
Machine root angle	353° 17′	73° 26′
Machine center to back	MD +1.34 mm	MD + 5.87mm
Sliding base (withdraw)	19.78 mm	0.00 mm
Blank offset	(up) 20.91 mm	0.00 mm
Eccentric angle	64° 29′	64° 33′
Cradle angle	355° 53′	122° 20′
Swivel angle	359°30′	310° 57′
Cutter spin. rot. ang.	52° 41′	0° 00′
Nc/50 ratio gears	53/42 * 48/76	
Helical motion gears	52/66 * 82/49	
Cutter diameter	9.075 in.	9.000 mm
Outside blade angle	17° 00′	17° 00′
Inside blade angle	28° 00′	18° 00′
Blade edge radius	0.060 in.	0.000 in.
Point width	0.124 in.	0.160 in.

0 20
(mm)
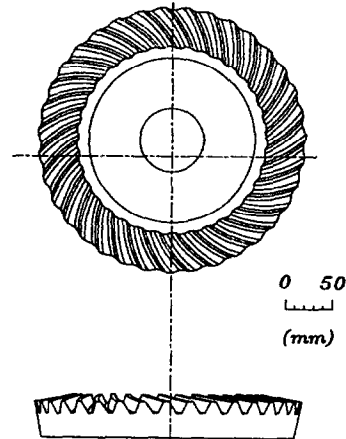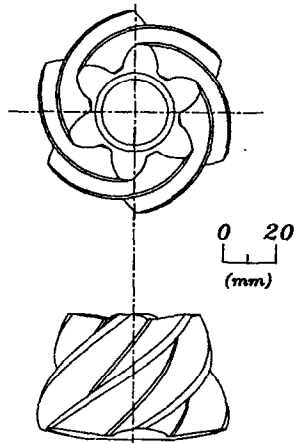
Figure 5. Tooth profile of hypoid pinion.

0 50
(mm)

Figure. 6. Tooth profile of hypoid gear.

7. CONCLUSION

The proposed mathematical model of the hypoid gear can be applied to simulate many different manufacturing methods for both spiral bevel gears and hypoid gears. It can also be applied to both the generated and nongenerated methods. There are four independent modules in the proposed mathematical model that benefit the coding of the computer program.

Based on the proposed mathematical model, the profile and surface coordinates of the hypoid pinion and gear can be obtained. In addition, the tooth contact analysis, kinematic error analysis, dynamic analysis and tooth geometry optimization can also be investigated.

REFERENCES

1. F.L. Litvin and Y. Gutman, Methods of synthesis and analysis for hypoid gear-drives of 'Formate' and 'Helixform', *J. Mech. Des.* **103**, 83–113 (1981).
2. L.E. Wilcox, A new method for analyzing gear tooth stress as a function of tooth contact pattern shape and position, *AGMA* (229.25) (1982).
3. R.L. Huston, Y. Lin and J.J. Coy, Tooth profile analysis of circular-cut spiral-bevel gears, *ASME J. Mech. Trans. Auto. Des.* **105**, 132–137 (1983).
4. F.L. Litvin, W.J. Tsung, J.J. Coy and C. Heine, Method for generation of spiral bevel gears with conjugate gear tooth surfaces, *ASME J. Mech. Trans. Auto. Des.* **109**, 163–170 (1987).
5. F.L. Litvin, Y. Zhang, M. Lundy and C. Heine, Determination of settings of a tilted head cutter for generation of hypoid and spiral bevel gears, *ASME J. Mech. Trans. Auto. Des.* **110**, 495–500 (1988).
6. Z.H. Fong, Tooth contact analysis and optimization of spiral bevel gears, Ph.D. Thesis, National Chiao Tung University, Taiwan, (1990).
7. Z.H. Fong and C.B. Tsay, A mathematical model for the tooth geometry of circular-cut spiral bevel gears, *ASME J. Mech. Des.* **113**, 174–181 (1991).
8. Z.H. Fong and C.B. Tsay, A study on the tooth geometry and cutting mechanisms of spiral bevel gears, *ASME J. Mech. Des.* **133**, 364–351 (1991).
9. F.L. Litvin, Theory of Gearing, NASA, Washington, D.C., (1989).
10. Gleason Works, *Gear Process Theory*, Rochester, NY.